Elite Master's Programme in Advanced Materials and Processes

Miniproject Report

Summer Semester 2017

Self-Assembly of Core-Shell nanoparticles

This miniproject is in partial fulfilment (8 ECTS) of the M4 Module in the focal subject "Computational Material Science and Process Simulation"

Student's Name	Trunov, Mikhail
Matriculation Number	22245933
Senior Supervisor	Prof. Dr. rer. nat. Michael Engel
Direct Supervisor (where applicable)	
Institute where miniproject was carried out	MSS

Abstract

Core-shell nanoparticles have been extensively studied as potential candidates for a wide range of applications, including bioimaging, sensors, thermometry and more in recent years. Typically a core-shell nanoparticle has a multi-layered structure, consisting of a host core covered by one or several shells. Improvements in computer performance contributed to advances in the behavior of many body particle systems research. The simulation of core-shell nanoparticles has recently revealed interesting 2D structures that particles arrange in, which motivated this work to computationally study many body core-shell nanoparticle systems behavior in three dimensions.

The present work employs event-driven molecular dynamics to study core-shell particle self-assembly. Two simulation approaches are performed. In the first approach the shell potential is slowly being increased while shell-to-core ratio and packing density are kept constant. In the second approach a range of shell-potential vs packing density combinations is simulated at three different shell-to-core ratios. Two new particle crystal configurations are discovered. The first configuration represents modulated body-centered cubic structure. The second found configuration is an icosahedral quasi-crystal.

I hereby declare that this project report is my own work, that I have only made use of the cited and/or acknowledged documents/resources and that this report has not been previously submitted as academic coursework elsewhere.

Erlangen, 29.09.2017	

Elite Master's Programme in Advanced Materials and Processes

Miniproject Report

Summer Semester 2017

Self-Assembly of Core-Shell nanoparticles

Grading Sheet

This miniproject is in partial fulfilment (8 ECTS) of the M4 Module in the focal subject "Computational Material Science and Process Simulation"

Student's Name	Trunov, Mikhail
Matriculation Number	22245933
Grade awarded:	
Comments:	

City, Date	Signature of supervising professor or lecturer with permission to examine

Note to grader: Please fill in and sign this form and return by mail or electronically to Dagmar Senft (MAP Office or dagmar.senft@fau.de) within 1 month after the submission.

1 Introduction

As pointed out by Whitesides and Grzybowski [1] the interest in self-assembly (SA) phenomenon is powered by a range of reasons – from the scientific prospective SA can help understand life and improve the knowledge of the connection between systems and their components, while from the technological view SA appears to be a natural manufacturing approach. The term self-assembly does not have a formal definition, [1] however according to the studies of Halley and Winkler [2] as well as Herr [3] SA is the non-dissipative process, involving spontaneous organization of (usually microscopic) self-assembling units into complex macroscopic structures, which were not present in the system before. Self-assembling units can be represented by nanoparticles, [4,5] block-copolymers, [6] various molecules, including peptides, [7] DNA, [8,9] nanoparticles with DNA ligands [10] and many more. Self-assembly of nanoparticles can lead to the emergence of materials with unique optical, [11] catalytic [12] and many other properties. The potential applications of self-assembled materials are biosensors, [13] drug delivery [14] and more. A comprehensive review on the self-assembled nanoparticle structures synthesis, properties and applications was recently published by Boles et al. [15]

The ordered structures of self-assembled nanoparticles can be interesting both from scientific and technological side. First, identifying regular shapes, that nanoparticles arrange in, it is possible to determine the space-fitting units – basic structures that can fill space, leaving no unoccupied regions, which is referred as tiling. Secondly, the unique structure can define valuable properties. The most intuitive way to tile space is to translate some pattern in non-parallel directions the number of which equals the number of considered space dimensions. The obtained ordered system is referred as periodic crystal structure. However, other ways to tile space with repeating units are possible. If the obtained structures are not periodic but still ordered they are called quasiperiodic. The most know examples of quasiperiodic structures or quasicrystals (QS) are Penrose tilings, which emerged from theoretical investigations. Real-life examples of QCs are usually found in metallic alloys, [16] while the number of experimental observations of soft matter QCs [17,18] is rather low. In quasiperiodic order space is tiled with a defined set of various shaped units called prototiles. As shown in the review of Zhang et al. [19] the synthesis of such prototiles is a possible task, as numerous number of experimentally observed various shaped crystals is reported. In the recent work of Damasceno et al. [20] the authors studied space tiling of 145 various polyhedra crystals via Monte Carlo simulations and characterized the observed results into four categories.

An important driving force of nanoparticle self-assembly is entropy, which for some cases is higher for ordered systems, than for disordered ones. Such concept does not seem intuitive, and in fact, as pointed out by Frenkel [21] only after 1957 hard sphere spontaneous freezing became a recognized fact due to the experimental evidence and theoretical rationalization.

Self-assembly behavior of nanoparticles is determined by their interaction and surrounding conditions. DLVO theory describes nanoparticle interactions in colloidal systems and considers van der Waals and electrostatic forces between nanoparticles, however Grasso et al. [22] pointed out that for some cases DLVO theory should be significantly extended by other inter-particle forces. The complexity of nanoparticle interactions as well as potential problems of creating particular environment makes it more feasible to study space tiling by nanoparticles via simulations rather than through experimental investigations.

The consideration of all the inter-particle forces is sometimes computationally too expensive, thus idealized models of interacting particles are proposed. The models typically include pair and cluster potentials as well as pair and cluster functionals. The simplest and computationally cheapest model is pair potential. The examples of particle self-assembly simulations include core-shell, [23–25] Dzugutov, [26] Morse [27] and other pair potentials.

Despite simplicity and low number of tunable parameters core-shell potential approximation contributed to the determination of a large number of various structures. [23] Particles, possessing core-shell potential behavior can be thought of as nanoparticles with metal or semiconductor hard cores with attached polymer ligands. An example of the experimental research of such system was reported by Hui et al. [28]

As shown by several numerical and experimental studies hard bodies like spheres [29] or polyhedra [20] can self-assemble into complex structures. The hard-body behavior can be easily obtained varying shell potential strength. Hence, when shell potential is weak, spherical core-shell nanoparticles behave as hard spheres with core radius, while when shell potential is strong, core-shell spherical nanoparticles behave as shell-radius hard objects.

Although the two dimensional core-shell nanoparticle self-assembly is well researched, the for-

mation of three dimensional self-assembled structures is not covered in literature. Hence at present no 3D simulations of core-shell nanoparticles were reported. Thus the present work aims to computationally study self-assembly of core-shell nanoparticles in three dimensions. Two main simulation approaches are used. The first approach is aimed to study the behavior of hard spheres. During the simulations the nanoparticle shell potential is slowly being increased. Experimental representation of such situation can be thought of as slowly increasing the nanoparticle surface coverage by ligands, which can be performed by increasing the ligand concentration in the nanoparticle solution. The purpose of the second simulation approach was to study core-shell nanoparticle behavior in an isolated system. Hence all the parameters, describing particle properties and environment were kept constant.

2 Simulation and methods

2.1 Simulation setup

The evolution of particle system was investigated via an event-driven molecular dynamics method. Each simulation was run on an ensemble of 2000 core-shell particles in a box with periodic boundary conditions at each boundary. The average kinetic energy of particles was maintained constant using velocity rescaling. Hence, the expression $k_B \cdot T = 1$ was maintained through all simulations. The core-shell pair potential between interacting particles was determined by:

$$U(r) = \begin{cases} 0, r \geq \lambda R_{core} \\ \epsilon, R_{core} < r < \lambda R_{core} \\ \infty, r \leq R_{core} \end{cases}, \tag{1}$$

here R_{core} – core radius, ϵ – shell potential value, λ – shell to core ratio. The packing density value was calculated only considering hard particle cores via:

$$\eta = \frac{4\pi \sum_{i=1}^{2000} R_{core}^3}{3V_{box}}, \tag{2}$$

where V_{box} denotes the simulation box volume.

The system evolution was analyzed in terms of event-driven molecular dynamics time units. The time unit was considered to be equal to 1. The times between events were calculated using conventional event-driven molecular dynamics approach.[30]

Two simulation approaches were implemented. In the first approach for each simulation the shell to core ratio and packing density were kept constant, while the shell potential was slowly being linearly increased (density vs shell-to-core ratio simulation). The simulation was run for each pair in the ranges 1.15–1.6 and 0.2–0.6 for shell-to-core ratio and packing density respectively. The step in both ranges was 0.05. The step at which shell potential was being increased as well as the maximum and the minimum considered values of shell potential were chosen individually for every packing density and shell-to-core ratio combination. At each shell potential value the system was given at least 50 event-driven molecular dynamics time units to equilibrate. At least 750 event driven molecular dynamics time units were performed in each simulation.

During another simulation approach all the parameters, including shell potential were kept constant, thus implementing NVT ensemble simulation. Three values of shell-to-core ratio were considered in the current work. For every shell-to-core ratio the simulations were performed in the ranges of 0.5–5 and 0.25–0.55 with incrementing steps of 0.5 and 0.01 for shell potential and packing density respectively. The results were summarized into packing density vs shell-potential phase diagrams for each shell-to-core ratio. The phases on the diagrams are marked with colors. White regions on diagrams mean the phase composition there was not determined and additional simulations are required. Due to limited time each simulation was run once covering at minimum 50 000 event driven molecular dynamics time units.

2.2 Methods

The present work employed methods described in the study of Engel et al.[31] Namely, radial distribution function, diffraction patterns and bond order diagrams were used to investigate the

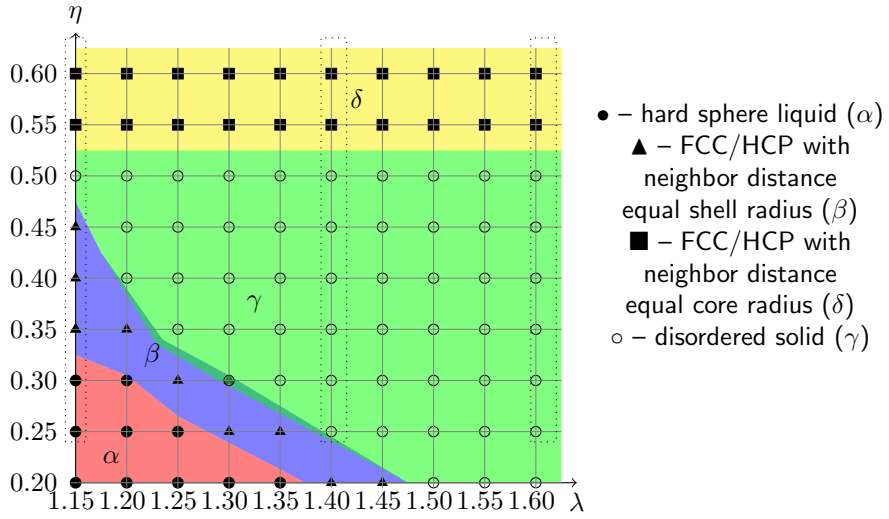

Figure 1: Packing density vs shell-to-core ratio phase diagram. The shell potential is slowly being increased during the simulation

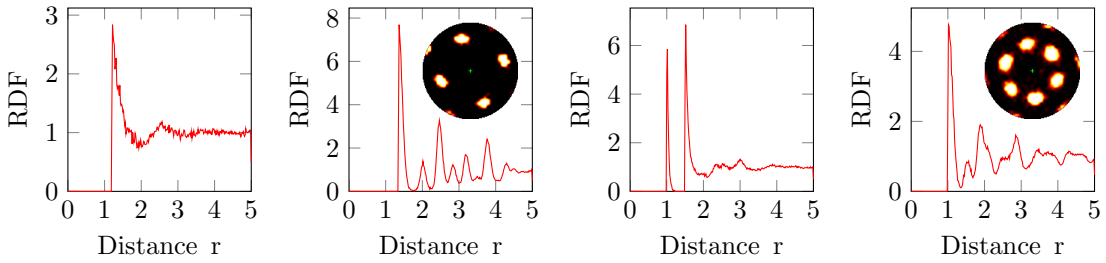

(a) α phase **(b)** β phase **(c)** γ phase **(d)** δ phase

Figure 2: Typical radial distribution functions and bond order diagrams (for β and δ phases) for simulations with increasing shell potential

order of self-assembled structures. Due to reasons discussed by Damasceno et al.[20] here I will not distinguish between FCC and HCP phases.

Radial distribution function (RDF) represents the average particle density at some distance from every particle in the simulation box. It helps to identify long range order in the researched system.

The diffraction patterns of the studied system were obtained by Fourier transform calculations of the particle projections along a chosen axis onto a plane. Each such projection represented a narrow Gaussian distribution. The method simulates electron diffraction experimental material investigations.

The bond orientation order diagrams are the distribution of the bond directions of the closest to a particle neighbors. The distributions are projected onto a sphere surface.

3 Results and Discussion

3.1 Density vs shell-to-core ratio simulations

The simulation with increasing shell potential value revealed the existence of four phases in the studied system (**Figure** 1). As seen from the RDF shapes (**Figures** 2a and 2b) particles in α and β phases behave as hard spheres of the shell-size radius. The α phase represents disordered hard-sphere liquid, while the β phase has an ordered FCC/HCP structure, which can be seen from its bond order diagram on the **Figure** 2b. The increase in the value of shell potential for α and β phases results in the potential energy / ϵ decline to zero (**Figure** 3a), which apparently determines the system equilibrium.

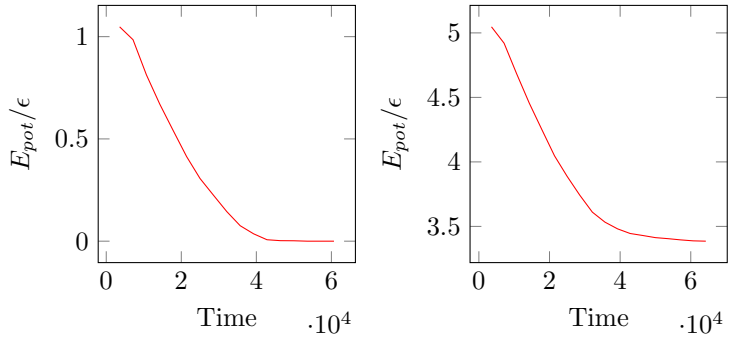

(a) for α and β phases **(b)** for γ and δ phases

Figure 3: Typical curves of the potential energy (E_{pot}) over shell potential ϵ evolution vs time for simulations with increasing shell potential

High packing density forces particles in γ and δ phases to penetrate into the shells of their neighbors, which is seen in the radial distribution functions behavior (**Figures** 2c and 2d). No order was observed for the γ phase region, while particles in the δ phase were organized into FCC/HCP with neighbor distance equal core radius crystals (**Figure** 2d). The potential energy over shell potential of the system for γ and δ phases decreased linearly until reaching constant level with the time (**Figure** 3b).

The observed data suggests that particles start to behave as hard bodies and self assemble into close packed structures when packing density reaches the 0.53–0.55 range. The FCC/HCP with neighbor distance equal shell radius structure was observed for packing density 0.53–0.68 considering density was calculated using shell radius. Same tendency to form FCC/HCP with neighbor distance equal core radius structure was observed for δ phase when the core packing density reached 0.52–0.55 range.

3.2 Packing density vs shell potential simulations

Basing on the previous studies of 2D systems[25,32] it can be concluded that some interesting structures can self-assemble only in a small range of temperatures and packing densities. Besides, not all shell-to-core ratios contribute to the formation of the rotational order. Taking everything above into account subsequent simulations were performed at constant shell potential and packing density with three shell-to-core ratio values — $\frac{2}{\sqrt{3}} = 1.1547, \sqrt{2} = 1.4142, \frac{\sqrt{8}}{3} = 1.633$. The investigated regions are marked with dashed lines on the **Figure** 1.

3.2.1 The 1.1547 shell-to-core ratio

The value of $\frac{2}{\sqrt{3}} = 1.1547$ was chosen as it resembles the distance ratio between next-nearest and nearest neighbors in BCC. The obtained results of the simulation are summarized as phase diagram in the **Figure** 6. As seen from the diagram three phases can be distinguished — disordered liquid, hard-sphere FCC and BCC.

Modulated BCC** phase was observed at high values of packing density and shell potential.The part of the phase diagram where BCC** was observed is shown in the **Figure** 4. Here each cross on the phase diagram represents one simulation. The initially formed BCC structure transformed into a more ordered system. The formation of the BCC** phase was observed when the potential energy vs simulation time curve changed the decline shape (**Figure** 5b). The RDF evolution during BCC to BCC** transition clearly identifies the emergence of higher order among the particle neighbors, lying in 1.5–2.2R_{core} distance range (**Figure** 5c). The comparison of bond order diagrams for BCC and BCC** phases suggests that each BCC bond direction distribution splits in at least seven smaller distributions.

The structure of the obtained BCC** phase has body centered nature, however the BCC unit cells are slightly deformed. The similarly deformed cells are apparently arranged into some order. The combination of BCC order and the order of equally deformed cells results in the emergence of the observed structure. The **Figure** 5a shows the distribution of the bond directions over the

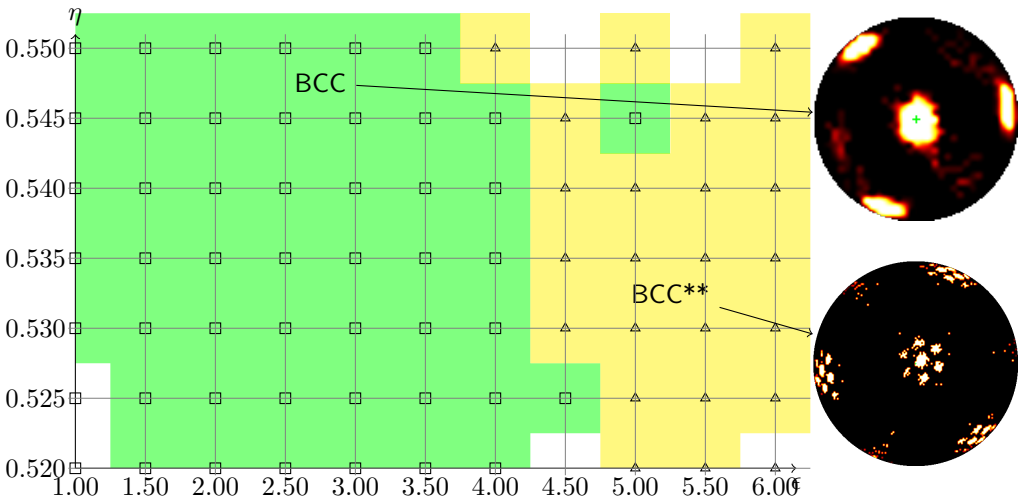

Figure 4: Phase diagram packing density η vs potential ϵ at constant $\lambda = 1.1547$ with bond order diagrams of the formed phases

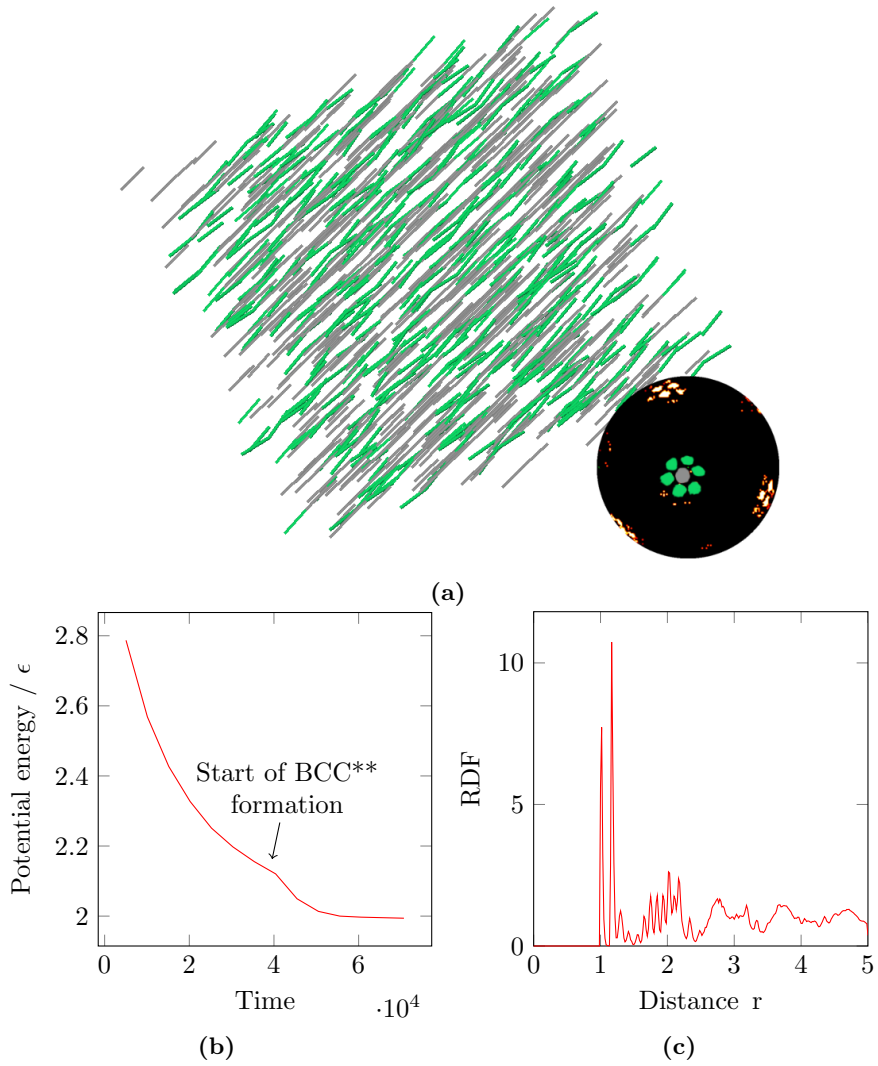

Figure 5: The BCC** structure describing parameters: a – BCC** bonds distribution, b – typical curve of the evolution of potential energy / ϵ vs time during the formation of BCC** structure and c – typical RDF shape

crystal. The bond colors correspond to the color on the bond order diagram. Hence the **Figure** 5a demonstrations the existence of some order between gray and green bonds.

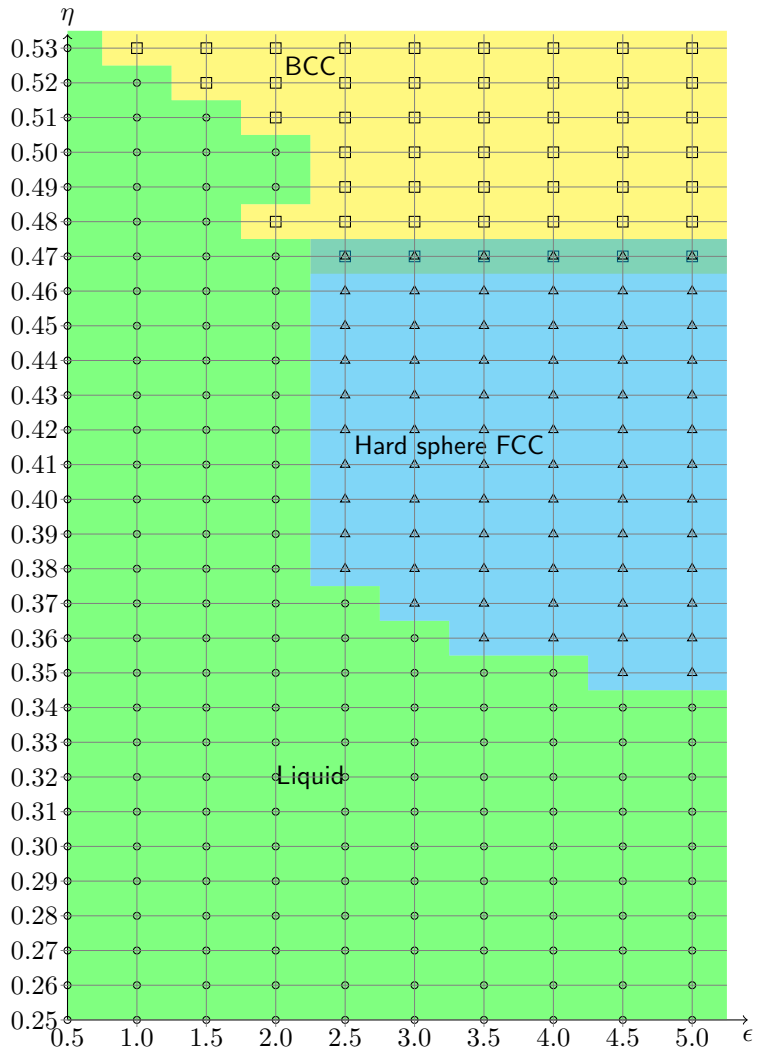

Figure 6: Phase diagram packing density η vs shell potential ϵ at constant $\lambda = 1.1547$

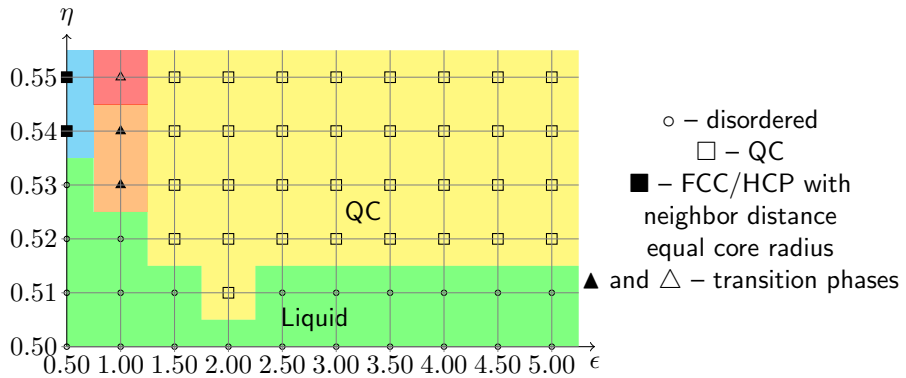

Figure 7: Phase diagram packing density η vs shell potential ϵ at constant $\lambda = 1.4142$

3.2.2 The 1.4142 shell-to-core ratio

Several studies[23,25] reported the existence of 2D quasi-periodic structures for the shell-to-core ratio of $\sqrt{2}$ which was a motivation to explore the $\sqrt{2}$ shell-to-core ratio in greater detail for 3D

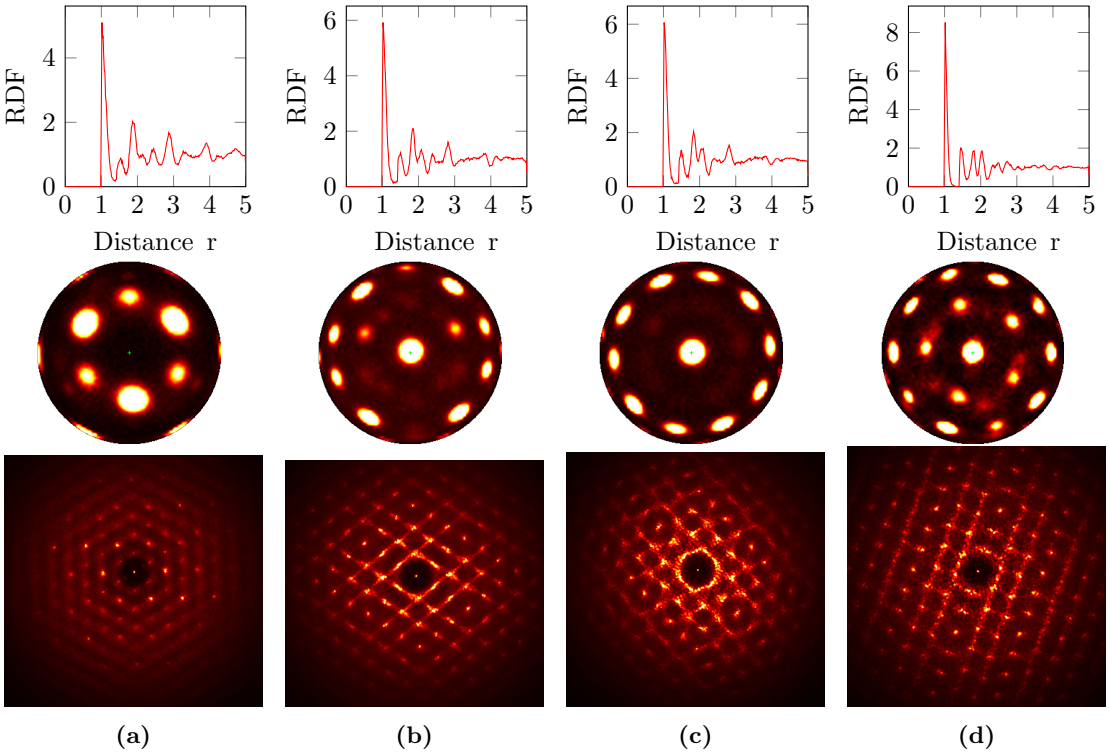

Figure 8: Radial distribution functions, bond order diagrams and diffraction patterns of the structures, formed at constant $\lambda = 1.4142$. a – FCC/HCP structure, formed at $\eta = 0.54$ and $\epsilon = 0.5$, b – transition structure, formed at $\eta = 0.54$ and $\epsilon = 1.0$, c – another transition structure, formed at $\eta = 0.55$ and $\epsilon = 1.0$ and d – QC structure, formed at $\eta = 0.53$ and $\epsilon = 3.5$

simulations.

Five phases were identified for the considered in the study $\eta-\epsilon$ range for $\lambda = 1.4142$ – disordered liquid, FCC/HCP with neighbor distance equal core radius, QC, and two transition phases. No ordered structure was observed in the 0.25–0.50 packing density range. Hence the range is not included into the obtained $\eta - \epsilon$ phase diagram which is shown in the **Figure** 7.

FCC/HCP structure forms at low values of shell potential. The increase in the shell potential forces particles to create transition structures. Two transition structures were recorded during my simulations. The first and the second structures, shown in the **Figures** 8b and 8c respectively have a very similar to FCC/HCP RDF shape. The second structure apparently has a 10-fold symmetry. The formation of the transition structures is accompanied by the reduction of the 3rd peak on FCC/HCP RDF. In the final QC structure the 2nd, 3rd and 4th peaks on RDF have equal height. Basing on the RDFs from the **Figure** 8 it can be concluded that the QC forms as a result of the particle rearrangement to a closer packed structure, hence the RDF 3rd peak located at about $1.9R_{core}$ distance reduces its height, which apparently results in the 2nd peak at about $1.5R_{core}$ distance growth. The moving particles change bond orientations, which is seen from the bond order diagrams.

Stereographic projections of the bond order diagrams of the obtained QC structure together with the previously reported in the studies of Engel et al.[31] and Damasceno et al.[33] icosahedral QSs are shown in the **Figure** 9. The shown in the **Figure** 9d QC structure is similar to the 9c, however the RDF and the diffraction pattern appear to be different from previously published results. The QC phase is stable in a large range of varied parameters, however at high shell potential values the QC structure becomes very defective.

3.2.3 The 1.633 shell-to-core ratio

The ratio of the axes in an ideally dense hexagonal packing equals $\frac{\sqrt{8}}{3} = 1.633$, which became the motivation to use this number as a shell-to-core ratio in the simulations.

No ordered phase was observed for all the considered in this work packing density values in the range from 0.25 to 0.52.The obtained phase diagram is shown in the **Figure** 10. The disordered

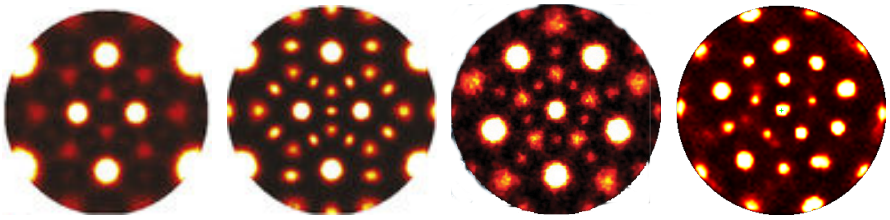

(a) (b) (c) (d)

Figure 9: Comparison between bond order stereographic projections. Here a, b and c are the projections of icosahedral QCs, obtained in the recent studies,[31,33] d — the QC projection from this work for the parameters $\lambda = 1.4142$, $\eta = 0.53$, $\epsilon = 3.5$

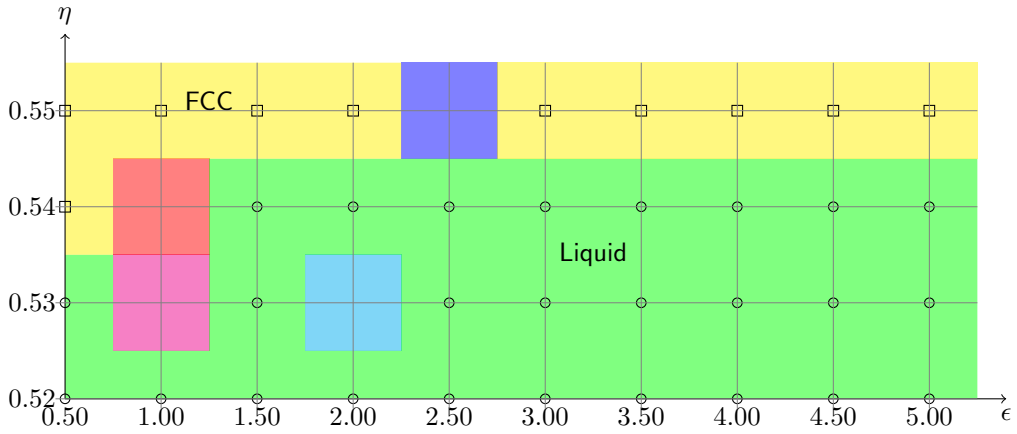

Figure 10: Phase diagram packing density η vs shell potential ϵ at constant $\lambda = 1.633$

phase in the 0.25-0.51 packing density range is not included.

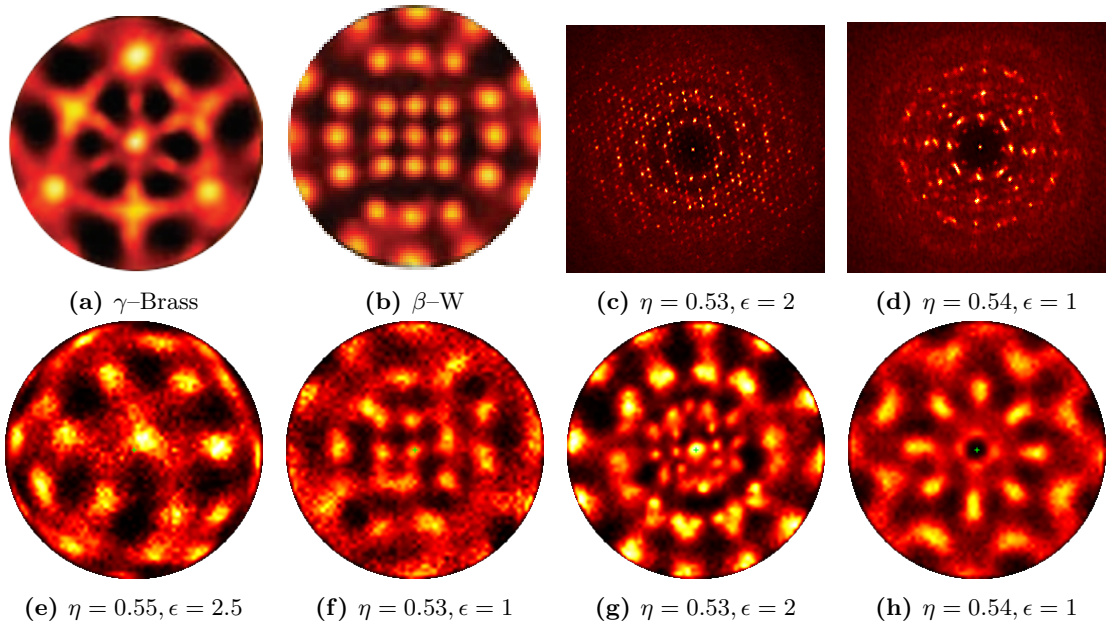

(a) γ–Brass **(b)** β–W **(c)** $\eta = 0.53, \epsilon = 2$ **(d)** $\eta = 0.54, \epsilon = 1$

(e) $\eta = 0.55, \epsilon = 2.5$ **(f)** $\eta = 0.53, \epsilon = 1$ **(g)** $\eta = 0.53, \epsilon = 2$ **(h)** $\eta = 0.54, \epsilon = 1$

Figure 11: Bond order diagrams and diffraction patterns, observed during simulations at constant $\lambda = 1.633$. a and b – previously reported bond order diagrams, c, d, e, f, g and h – diffraction patterns and bond order diagrams observed in this work.

At the packing density of 0.55 the diagram is mostly occupied by FCC, however in very small regions the emergence of QC phase is also possible. Thus at $\epsilon = 2.5$, $\eta = 0.55$ and $\epsilon = 1$, $\eta = 0.53$

γ-brass and β–W phases were observed respectively. Previously reported as well as observed in this work bond order diagrams for the γ-brass and β–W phases [20] are shown in the **Figures** 11a, 11e, 11b and 11f.

The bond order diagrams as well as the diffraction patterns of the structures, that were not identified by me in the previously published works are shown in the **Figures** 11c, 11d, 11g and 11h.

4 Conclusion

Two new configurations in which core-shell particles arrange in space were discovered in this study. The first configuration was observed for the shell-to-core ratio of 1.1547. The configuration represents a more complex form of a BCC structure. Equally deformed BCC unit cells arrange in an ordered pattern, which is thermodynamically more favorable for the system rather than BCC. The second configuration found in this work is apparently an icosahedral quasi-crystal. The QC was observed for close to $\sqrt{2}$ shell-to-core ratios. The evolution of FCC transformation into QC was discussed.

Several crystal configurations were reproduced in this study. The crystal configurations observed here for shell-to-core ratio of 1.633 were previously found by Damasceno et al. [20] However the authors simulated hard polyhedra particles instead of core-shell spherical ones.

The first employed here simulation approach with slowly increasing shell potential value helped to identify the regions where particles behave as hard spheres either of shell or core radius. Identical packing density values of 0.53-0.55 were observed for the core radius and the shell radius nanoparticles when they started behaving as ordered hard spheres.

The second simulation approach with fixed shell-to-core ratio is better at phase identifications, but the approach is slower as it requires to iterate through the three parameters.

Based on the obtained results there are still several unanswered in this work questions, which can be addressed in the future research. Hence the order of the space positions of deformed BCC unit cells in BCC** phase was not determined. Besides a proper analysis of QC structures obtained at 1.4142 shell-to-core ratio should be performed. The detailed structure analysis should also be performed for the QCs found at 1.633 shell-to-core ratio. Another potential research direction is the refinement of the discovered here phase boundaries. Hence the transition phases found at $\lambda = 1.4142$ simulations seem to occur in a rather small shell potential range. The detailed determination of the phase boundaries could be further investigated.

Acknowledgments

I would like to thank my supervisor Professor Michael Engel for the support, all the provided to me resources and wonderful experience of participation in the life of his team and the Institute for Multiscale Simulation. I would like to acknowledge Marco Klement for help with technical issues.

References

[1] Whitesides, G. M.; Grzybowski, B. Self-Assembly at All Scales. *Science* **2002**, *295*, 2418–2421.

[2] Halley, J. D.; Winkler, D. A. Consistent concepts of self-organization and self-assembly. *Complexity* **2008**, *14*, 10–17.

[3] Herr, D. J. Directed block copolymer self-assembly for nanoelectronics fabrication. *Journal of Materials Research* **2011**, *26*, 122–139.

[4] Grzelczak, M.; Vermant, J.; Furst, E. M.; Liz-Marzán, L. M. Directed Self-Assembly of Nanoparticles. *ACS Nano* **2010**, *4*, 3591–3605.

[5] Nie, Z.; Petukhova, A.; Kumacheva, E. Properties and emerging applications of self-assembled structures made from inorganic nanoparticles. *Nature nanotechnology* **2010**, *5*, 15–25.

[6] Mai, Y.; Eisenberg, A. Self-assembly of block copolymers. *Chemical Society Reviews* **2012**, *41*, 5969–5985.

[7] Hamley, I. W. Self-assembly of amphiphilic peptides. *Soft Matter* **2011**, *7*, 4122–4138.

[8] Saccá, B.; Niemeyer, C. M. DNA Origami: The Art of Folding DNA. *Angewandte Chemie International Edition* **2012**, *51*, 58–66.

[9] Wilner, O. I.; Willner, I. Functionalized DNA Nanostructures. *Chemical Reviews* **2012**, *112*, 2528–2556.

[10] Mirkin, C. A.; Letsinger, R. L.; Mucic, R. C.; Storhoff, J. J. A DNA-based method for rationally assembling nanoparticles into macroscopic materials. *Nature* **1996**, *382*, 607–609.

[11] Kuzyk, A.; Schreiber, R.; Fan, Z.; Pardatscher, G.; Roller, E.-M.; Hogele, A.; Simmel, F. C.; Govorov, A. O.; Liedl, T. DNA-based self-assembly of chiral plasmonic nanostructures with tailored optical response. *Nature* **2012**, *483*, 311–314.

[12] Miao, X.; Cao, W.; Zheng, W.; Wang, J.; Zhang, X.; Gao, J.; Yang, C.; Kong, D.; Xu, H.; Wang, L.; Yang, Z. Switchable Catalytic Activity: Selenium-Containing Peptides with Redox-Controllable Self-Assembly Properties. *Angewandte Chemie International Edition* **2013**, *52*, 7781–7785.

[13] Sun, H.; Li, W.; Wu, L. Honeycomb-Patterned Films Fabricated by Self-Organization of DNA-Surfactant Complexes. *Langmuir* **2009**, *25*, 10466–10472.

[14] Karagoz, B.; Esser, L.; Duong, H. T.; Basuki, J. S.; Boyer, C.; Davis, T. P. Polymerization-Induced Self-Assembly (PISA)–control over the morphology of nanoparticles for drug delivery applications. *Polymer Chemistry* **2014**, *5*, 350–355.

[15] Boles, M. A.; Engel, M.; Talapin, D. V. Self-Assembly of Colloidal Nanocrystals: From Intricate Structures to Functional Materials. *Chemical Reviews* **2016**, *116*, 11220–11289, PMID: 27552640.

[16] Kim, Y. K.; Kim, W. T.; Kim, D. H. Quasicrystal-reinforced Mg alloys. *Science and Technology of Advanced Materials* **2014**, *15*, 024801.

[17] Zeng, X.; Ungar, G.; Liu, Y.; Percec, V.; Dulcey, A.; Hobbs, J. K. Supramolecular dendritic liquid quasicrystals. *Nature* **2004**, *428*, 157.

[18] Talapin, D. V.; Shevchenko, E. V.; Bodnarchuk, M. I.; Ye, X.; Chen, J.; Murray, C. B. Quasicrystalline order in self-assembled binary nanoparticle superlattices. *Nature* **2009**, *461*, 964.

[19] Zhang, L.; Niu, W.; Xu, G. Synthesis and applications of noble metal nanocrystals with high-energy facets. *Nano Today* **2012**, *7*, 586 – 605.

[20] Damasceno, P. F.; Engel, M.; Glotzer, S. C. Predictive Self-Assembly of Polyhedra into Complex Structures. *Science* **2012**, *337*, 453–457.

[21] Frenkel, D. Order through entropy. *Nature materials* **2015**, *14*, 9–12.

[22] Grasso, D.; Subramaniam, K.; Butkus, M.; Strevett, K.; Bergendahl, J. A review of non-DLVO interactions in environmental colloidal systems. *Reviews in Environmental Science and Biotechnology* **2002**, *1*, 17–38.

[23] Dotera, T.; Oshiro, T.; Ziherl, P. Mosaic two-lengthscale quasicrystals. *Nature* **2014**, *506*, 208.

[24] Schoberth, H. G.; Emmerich, H.; Holzinger, M.; Dulle, M.; Forster, S.; Gruhn, T. Molecular dynamics study of colloidal quasicrystals. *Soft Matter* **2016**, *12*, 7644–7654.

[25] Pattabhiraman, H.; Gantapara, A. P.; Dijkstra, M. On the stability of a quasicrystal and its crystalline approximant in a system of hard disks with a soft corona. *The Journal of chemical physics* **2015**, *143*, 164905.

[26] Ryltsev, R.; Chtchelkatchev, N. Universal self-assembly of one-component three-dimensional dodecagonal quasicrystals. *Soft Matter* **2017**,

[27] Ye, X.; Chen, J.; Irrgang, M. E.; Engel, M.; Dong, A.; Glotzer, S. C.; Murray, C. B. Quasicrystalline nanocrystal superlattice with partial matching rules. *Nature materials* **2017**, *16*, 214–219.

[28] Hui, C. M.; Pietrasik, J.; Schmitt, M.; Mahoney, C.; Choi, J.; Bockstaller, M. R.; Matyjaszewski, K. Surface-Initiated Polymerization as an Enabling Tool for Multifunctional (Nano-)Engineered Hybrid Materials. *Chemistry of Materials* **2014**, *26*, 745–762.

[29] Tang, J.; Zhou, X.; Zhao, D.; Lu, G. Q.; Zou, J.; Yu, C. Hard-Sphere Packing and Icosahedral Assembly in the Formation of Mesoporous Materials. *Journal of the American Chemical Society* **2007**, *129*, 9044–9048, PMID: 17595080.

[30] Pöschel, T.; Schwager, T. *Computational granular dynamics: models and algorithms*; Springer Science & Business Media, 2005.

[31] Engel, M.; Damasceno, P. F.; Phillips, C. L.; Glotzer, S. C. Computational self-assembly of a one-component icosahedral quasicrystal. *Nature materials* **2015**, *14*, 109.

[32] Pattabhiraman, H.; Dijkstra, M. Phase behaviour of quasicrystal forming systems of core-corona particles. *The Journal of Chemical Physics* **2017**, *146*, 114901.

[33] Damasceno, P. F.; Glotzer, S. C.; Engel, M. Non-close-packed three-dimensional quasicrystals. *Journal of Physics: Condensed Matter* **2017**, *29*, 234005.